Inorganic Chemistry

ARTICLE

pubs.acs.org/IC

High Temperature NMR Study of Aluminum Metal Influence on Speciation in Molten NaF-AlF_3 Fluorides

Ioana Nuta,[†,‡,§] Emmanuel Veron,[†,‡] Guy Matzen,[†,‡] and Catherine Bessada*[,†,‡]

[†]CEMHTI, CNRS UPR 3079, 1D avenue de la recherche scientifique, 45071 Orléans cedex 2, France

[‡]Université d'Orléans, avenue du Parc Floral, BP 6749, 45067 Orléans cedex 2, France

ABSTRACT:

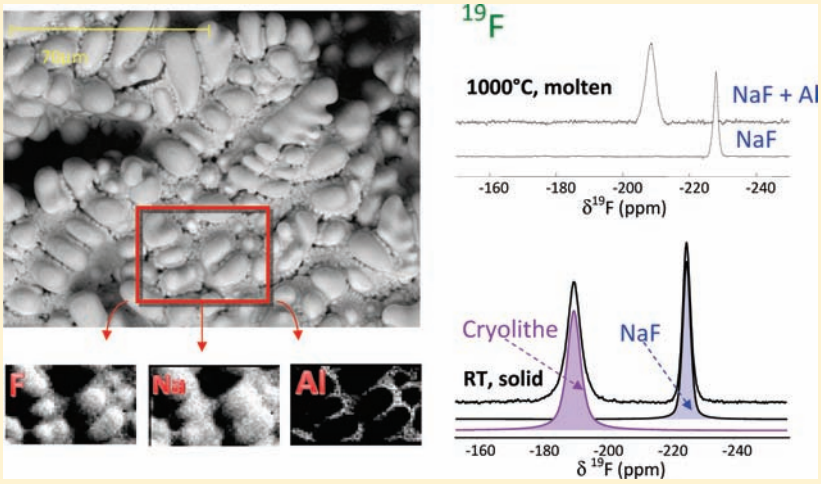

In situ high temperature NMR spectroscopy has been used to characterize the interactions between aluminum metal and cryolitic melts. ^{27}Al, ^{23}Na, and ^{19}F NMR spectra have been acquired in NaF-AlF_3 and NaF-AlF_3-Al melts over a wide range of compositions. The evolution of the signals evidence a chemical reaction between the metal and the salt. The different samples have been also described after solidification at room temperature by Environmental Scanning Electronic Microscopy, high resolution solid state NMR, and X-ray diffraction. The combination of in situ high temperature NMR characterization of the melts, with experimental description of solidified samples after cooling, evidence an enrichment of the melts with AlF_3 and different reactions with metallic aluminum depending on the initial bath composition.

1. INTRODUCTION

Aluminum is produced industrially by the Hall Heroult process. In this process, alumina is electrolytically reduced to aluminum metal and oxygen, in a bath containing mainly cryolite and different additives.[1,2] The density of molten aluminum is higher than the bath, and it falls to the bottom of the cell. Aluminum is then in contact with the carbon cathode, the bath, and the cell lining. This can induce loss of current efficiency by different negative reactions such as aluminum dissolution into the electrolyte, metal losses into the cell lining, or its contamination by sodium. These reactions may influence the distribution or the nature of the chemical species in the melt and thus the properties of the bath.

Previous experiments showed that when a piece of aluminum was added to NaF-AlF_3 melts a gray fog was formed above the liquid, while the melt itself became opaque.[3−9] This fog was observed with or without electrolysis and depending on the AlF_3 content. Different measurements of total vapor pressure[10,11] explained these vapors as being made of metallic sodium. This information was confirmed by Raman spectroscopy with the detection of sodium vapor over the melt.[12] Some authors[9] have detected metallic particles dispersed in the solid bath after its cooling, and it was concluded that such dispersions should be present in the melt before solidification. The size of such dispersions depends on the cooling rate and on the composition of the bath. The determination of the aluminum solubility has been approached by different methods such as the analysis of the metal after solidification, and by the weight loss calculations.[3−9] However, the data obtained are quite dispersed because of possible interactions between the aluminum and the crucible material or the atmosphere above the bath and because of the evaporation observed and invoked above.

The ionic structure of NaF-AlF_3 binary melts have been proposed by different authors.[1] The model involving three alumino-fluoride species AlF_4^-, AlF_5^{2-}, AlF_6^{3-} has been confirmed by high temperature Raman and NMR spectroscopy.[12,13]

Received: September 28, 2010
Published: March 17, 2011

Only minor amounts of AlF_6^{3-} species are detected over the entire range of composition while the AlF_5^{-} species become predominant around the cryolite (25 mol % AlF_3) composition.

For baths containing metallic aluminum only little structural information is available.[1] It is known that the metal dissolution in cryolitic melt is low (0.1 wt %), and depends on melts basicity, temperature, and on the nature of additives. It has been proposed that aluminum is present in the bath as aluminum dispersions, alumino-fluoride species, and under different oxidation states. Owing to experimental difficulties, these structural modifications are not clearly described, and are often based on simple observations and theoretical models.

In a previous paper,[14] we have presented preliminary results obtained by high temperature ^{27}Al, ^{23}Na, and ^{19}F NMR spectroscopy on the structural changes occurring with aluminum dissolution in NaF-AlF_3 molten mixtures. From the evolution of the NMR signals in the melts and the structural characterization of the solidified samples, we have proposed some modifications of the fluoroaluminate species distribution because of the reaction of aluminum with the bath and its enrichment in AlF_3.

In the present paper, we have analyzed an extended domain of NaF-AlF_3 compositions up to very low AlF_3 content with and without aluminum metal. A detailed analysis was also performed on pure NaF composition, from room temperature up to 1000 °C. To describe the phases formed on cooling after reactions at high temperature, the compositions were also characterized at room temperature after solidification using high resolution solid state NMR, Environmental Scanning Electron Microscopy, and X-ray diffraction.

2. EXPERIMENTAL SECTION

Samples. According to the phase diagram,[1] compositions ranging from 0 to 50 mol % AlF_3, were prepared by mixing suitable amounts of NaF (Sigma-Aldrich Co., 99.9%) and AlF_3 (Inland, 99.9%, purified by two sublimations at 1273K) powders. Natural cryolite from Ivigtut, Greenland was used for the 25 mol % AlF_3 composition. Small pieces (3 mg) of metallic aluminum of high purity (Rio-Tinto-Alcan) were added to 70 mg of each NaF-AlF_3 mixture into a boron nitride crucible tightly closed with a screwed cap. The boron nitride is of very high purity (BN AX05 MCSE), with a negligible amount of oxide binder, to limit any possible interactions with the fluoride bath. Samples preparation were made in a glove-box under dried argon (H_2O content <2 ppm, O_2< 4 ppm).

After high temperature NMR measurements, the solidified mixtures are first characterized without any preparation by Environmental Scanning Electronic Microscopic (ESEM). They are then crushed and characterized by Magic-Angle Spinning (MAS) NMR and X-ray Diffraction.

NMR Measurements. The high temperature NMR measurements were performed using the laser-heating system developed in Orléans.[15] The bottom of the crucible containing the sample is directly heated by a continuous CO_2 laser (λ = 10.6 μm, 120 W) axially through the NMR probehead. The temperature calibration was made using a calibration of the laser power with temperature measured by a K type thermocouple located inside a BN crucible filled with BN powder, for the same heating and cooling procedure than the experiments. The accuracy on temperatures is estimated within ±5 °C. BN crucibles are protected from oxidation at high temperature by a continuous argon flow. The electronics and the radio frequency coil are cooled by an air flow at room temperature. The ^{27}Al, ^{19}F, and ^{23}Na high temperature NMR spectra were acquired for each composition, 10 degrees above the corresponding melting temperature. A single pulse sequence was used for high temperature experiments with $\pi/8$ (for ^{27}Al and ^{23}Na) and $\pi/2$ (for ^{19}F) pulses, and recycle delays of 0.5 s for ^{27}Al and ^{23}Na and 5 s for ^{19}F. The obtained spectra at high temperature are sharp and well resolved. The acquisitions are short and require only 8 to 64 scans. Because fluoride melts are very corrosive and can be associated with a non congruent vaporization, the experimental time spent in the liquid phase has been minimized and is less than ≈15 min to avoid evolution of the composition during the experiments.

MAS NMR spectra were acquired at room temperature using a 2.5-mm Bruker High Speed MAS NMR probe with a spinning rate of 20 kHz. ^{27}Al and ^{23}Na spectra were collected using a **T**wo **P**ulse **P**hase **M**odulation (TPPM)[16,17] ^{19}F decoupling sequence to improve ^{19}F decoupling and spectra resolution. Spectra were simulated with the DMFit program.[18]

All NMR experiments were carried out on a Bruker Avance 400 spectrometer operating at 9.4T. ^{27}Al, ^{23}Na, and ^{19}F signals are referenced to $Al(NO_3)_3$, NaCl 1 M aqueous solutions, and pure $CFCl_3$ respectively.

ESEM Analysis. An FEI/Philips XL40 ESEM equipped with an energy dispersive X-ray spectrometer (EDS) was used for the samples characterization. Compared with conventional SEM, in Environmental Scanning Electron Microscopy (ESEM) non conductive materials can be imaged without any conductive coating, allowing a direct observation with no damage to the sample. Imaging was performed with a gaseous secondary electron detector (GSED), an accelerating voltage of 20 kV, and a water pressure of 0.3 Torr in the chamber. This low pressure was used to keep a good spatial resolution for the X-ray analysis by minimizing the scattering of the primary electrons beam.

The samples were inserted into the microscope chamber at room temperature after the high temperature NMR experiments.

X-ray diffraction analysis were done at room temperature under air on a Philips PW1729 diffractometer ($CuK\alpha_{1,2}$ radiation).

2. RESULTS AND DISCUSSIONS

2.1. Samples at High Temperature. *High Temperature NMR Study of NaF-AlF_3 System.* Figure 1 shows the chemical shifts evolution obtained for ^{27}Al, ^{23}Na, and ^{19}F, measured for NaF-AlF_3 compositions ranging from 0 to 50 mol % AlF_3 with and without aluminum metal. The values reported in this work for the system without metal addition are in good agreement with previous data obtained by Lacassagne et al.[13] from 20 to 50 mol % AlF_3. This work completes the domain of compositions up to low AlF_3 contents, unstudied until now. ^{27}Al chemical shifts increase with AlF_3 content over the whole range of compositions, while ^{23}Na chemical shifts decrease from 5 ppm in NaF to −17.6 ppm in $NaAlF_4$ (50 mol %AlF_3). ^{19}F chemical shifts range between −228 and −190 ppm with a plateau between cryolite and chiolite compositions. This confirms the "bell-shape"evolution for ^{19}F chemical shifts previously proposed by Lacassagne et al.[13]

The NMR signal obtained in a melt at high temperature is a single narrow line because of a rapid and dynamical exchange between the different species involving the observed nucleus. The peak position is the average between the chemical shifts of the different units present in the melt weighted by their relative proportions. If the bath is composed of different ionic species, A_i (e.g., F^-, AlF_4^-, AlF_5^{2-}, AlF_6^{3-}, etc.) the measured chemical shift of a N nucleus (e.g., ^{19}F, etc.), $\delta(N)$, can be expressed as

$$\delta(N) = \sum_i X_{A_i}^N . \delta^N(A_i)$$

where X_{Ai}^N is the atomic fraction of N in the A_i species and $\delta^N(A_i)$ is the chemical shift of N for A_i species.

dx.doi.org/10.1021/ic1019845 |*Inorg. Chem.* 2011, 50, 3304–3312

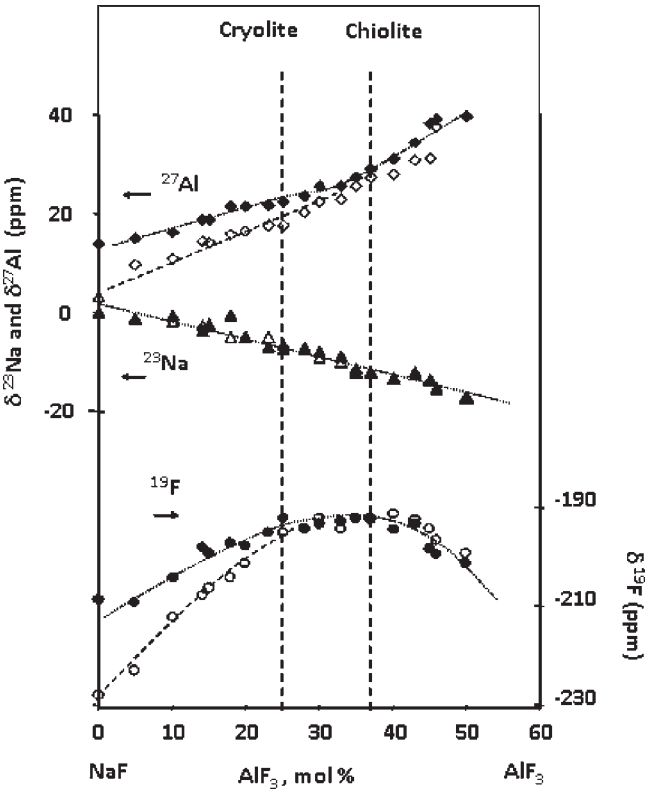

Figure 1. High temperature evolution of ^{27}Al, ^{19}F, and ^{23}Na chemical shifts in molten NaF-AlF_3 (empty symbols) and NaF-AlF_3-Al (filled symbols) systems.

In a first empirical approach, to deduce the anionic proportions from the measured ^{27}Al chemical shifts, we need to know the chemical shift value for each coordination. In solid alkali fluoroaluminates, aluminum atoms are essentially octahedrally coordinated with F, and the ^{27}Al chemical shifts range reported lies between −15 and +2 ppm.

We have selected the value measured in the high temperature solid phase of cryolite before the melting at 1253K ($\delta_{VI}^{Al} = 2$ ppm) because the local environment of the aluminum 6-coordinated in this high temperature phase is very close to the one in the melt.

For the AlF_5^{2-} chemical shift, only very rare data have been reported on 5-fold coordination. The value reported by Kohn et al.,[22] obtained in a jadeite glass doped with cryolite, and that obtained by Dirken et al[23] at 20 ppm are in good agreement with the values reported by Lacassagne et al.[13] in the molten state. The value considered for the AlF_4^- chemical shift is the value obtained in the melt at 50% mol AlF_3 (1303 K). At this composition it has been shown that only AlF_4^- species are present,[19] and the measured chemical shift is $\delta_{IV}^{Al} = 40$ ppm.

As it was proposed by Gilbert et al.,[19−21] the fluoroaluminate species present at low AlF_3 contents are mainly AlF_6^{3-} and AlF_5^{2-}, while the AlF_4^- species appear for content higher than 20 mol % AlF_3. In the range of composition concerned in our calculation (0−20 mol %), fluorine atoms are only involved in AlF_6^{3-}, AlF_5^{2-} complexes, and in free fluorine ions, F^-. Therefore, the ^{19}F chemical shift can be expressed as

$$\delta_F = X_{F^-}^F . \delta_{F^-}^F + X_{AlF_6^{3-}}^F . \delta_{VI}^F + \delta_{AlF_5^{2-}}^F . X_V^F$$

The ^{19}F chemical shift values are taken from Lacassagne et al.:[13] the value measured in pure molten NaF at −228 ppm

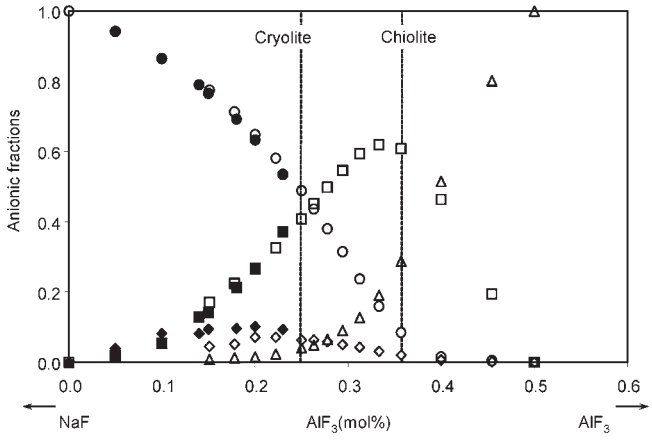

Figure 2. Anionic molar fractions of the different species present in melts of the NaF-AlF_3 system. *o* F-, Δ AlF_4^-, □ AlF_5^{2-}, ◊ AlF_6^{3-} (Filled symbols, this study; empty symbols, Raman data from Gilbert et al.[17−19]).

is assigned to the free fluorine ion. The chemical shifts for AlF_6^{3-} and AlF_5^{2-} were defined at $\delta_{VI}^{Fl} = -176$ ppm, and $\delta_V^F = -188$ ppm.

From the atomic fractions determined from the experimental chemical shift we can extract the anionic molar fractions with the equation

$$X_i = \frac{n_i^0}{\sum n_i^0}$$

where n_i^0 is the initial molar number of the *i*-th species.

Using the conservation rules for each atom of the system

Aluminum conservation: $[AlF_3]_0 = n_6 + n_5$.

Fluorine conservation: $3[AlF_3]_0 + [NaF]_0 = 6n_6 + 5n_5 + n_{F^-}$ and $n_T = n_6 + n_5 + n_{F^-}$.

We have reported in Figure 2 the anionic fractions given by our NMR data and the values deduced from the Raman experiments.[21] The anionic fractions calculated for the composition range 0−20 mol % AlF_3 shows an important contribution of AlF_5^{2-} and confirm the dissociation of AlF_6^{3-} in AlF_5^{2-} according to the model:

$$AlF_6^{3-} \leftrightarrow AlF_5^{2-} + F^-$$

followed for higher AlF_3 content by a further dissociation of AlF_5^{2-} in AlF_4^-.

$$AlF_5^{2-} \leftrightarrow AlF_4^- + F^-$$

already defended by Gilbert et al.[19−21,24−26] The slight difference observed between the two series of data between 15 to 20% mol AlF_3 can be explained by the presence of a small amount of AlF_4^- which is not taken into account in this calculation. Nevertheless, the agreement is quite satisfactory.

NMR Study of Aluminum Metal. NMR studies on metals are conditioned by the size of metallic particles in the sample. The radiofrequency field is able to go through the metallic species under 50 μm. If the sample is a piece of metal with higher dimensions, only the nuclei located in a layer of this thickness participate in the resonance and the resulting signal will be too weak to be detectable. This phenomenon is due to a specific property of metals called "skin effect" linked to the screening of the magnetic field by the conducting electrons. To improve the very weak NMR signal, a solution is to increase the ratio area/volume by using fine powders, or thin films. If the size of the

dx.doi.org/10.1021/ic1019845 |*Inorg. Chem.* 2011, 50, 3304–3312

sample is comparable with the depth of the skin, the NMR response will be very complex and not exploitable. Knight[27] has shown that the NMR signal of a metal is at higher frequency than the same nuclear species in a non metallic material. This shift, called "Knight Shift", is due to the hyperfine interactions between the nuclear moments and the electromagnetic field around the nuclei. The Knight shifts of metallic aluminum and sodium have been reported in metallic materials with cubic structure at 1640 ppm and 1120 ppm, respectively.[28,29]

To highlight the ^{27}Al NMR signature of the molten metal, 2 mg of aluminum powder ($\phi = 15\,\mu$m) was dispersed in an MgO powder. Figure 3 presents the comparison between the ^{27}Al NMR spectrum of molten aluminum registered at 973 K and the ^{27}Al MAS NMR spectrum of solid metal at room temperature. Chemical shifts are quite similar: 1640 ppm for solid metal and 1630 ppm for liquid aluminum.

For all samples studied in NaF-AlF_3-Al system, aluminum was introduced as pieces of few milligrams. It explains why the ^{27}Al signal of the metal was not detectable on the spectra of these compositions if no reaction occurred into the bath. Non reacted aluminum metal could not be detected by ^{27}Al NMR, and, conversely, if dispersions are formed and preserved on cooling, it would be possible to detect their NMR signature at room temperature.

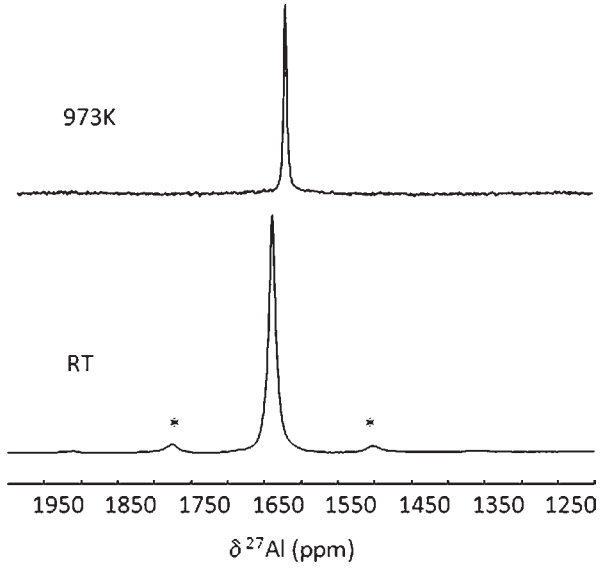

Figure 3. ^{27}Al NMR spectra of metallic aluminum powder dispersed in MgO powder. Comparison between ^{27}Al NMR spectrum for molten aluminum at 973 K (upper spectrum) and ^{27}Al MAS NMR for solid aluminum at room temperature (bottom spectrum). Asterisks, *, designate spinning sidebands.

High Temperature NMR Study of NaF and NaF+Al Metal. Figure 4 shows ^{19}F and ^{23}Na NMR spectra obtained for NaF sample at 1283 K for different heating durations. It was observed that the ^{19}F and ^{23}Na signals at −228 ppm and 5 ppm, respectively, are not modified during heating. The ^{19}F spectra recorded at 1283 K for NaF containing aluminum metal (Figure 5) shows a shift of 19 ppm and thus appears at −209 ppm. The signal is slightly shifted during heating, and it is stabilized at −206 ppm after 10 min. From the beginning of the heating of the sample with Al metal, the ^{23}Na spectrum is slightly broadened (350 Hz) compared with pure NaF (300 Hz). During the heating, the peak shifts up to 0 ppm because of the presence of Al metal. After 10 min at 1283 K (Figure 5), a small ^{27}Al NMR signal is detected at 14 ppm. This value coincides with the chemical shift values measured for fluoroaluminate species in molten NaF-AlF_3 melts with low AlF_3 content below 10 mol % (see Figure 1). This observation confirms the reaction between aluminum metal and molten NaF and the formation of AlF_3 in the melt.

High Temperature NMR Study of NaF-AlF_3-Al System. The chemical shifts obtained for the different NaF-AlF_3 compositions in this study were systematically compared with that acquired in the system with aluminum metal (Figure 1). The observed chemical shifts' behavior indicates that they depend strongly on the AlF_3 content. For ^{27}Al, and ^{19}F, it was remarked a systematic shift toward upper chemical shift values, while for ^{23}Na no evolution is visible when aluminum is added. This trend is clearly observed up to the cryolite composition, and is less visible for higher AlF_3 contents.

For fluorine, the same trend was observed than in the NaF-AlF_3 system but shifted toward higher chemical shifts for 0 to 25 mol % AlF_3 range. This shift decreases rapidly with AlF_3 contents. For compositions above 25 mol % AlF_3 no change was observed. The trends observed for ^{27}Al and ^{19}F mainly below 25 mol % AlF_3 correspond to the modification of the average local environment around fluorine and aluminum atoms when the aluminum metal reacts with the bath. When Al metal is added to the baths at low AlF_3 content (i.e., 0 to 15 mol % AlF_3 range), the ^{27}Al and ^{19}F chemical shifts are similar to values obtained for baths without metal but with higher AlF_3 content. This main

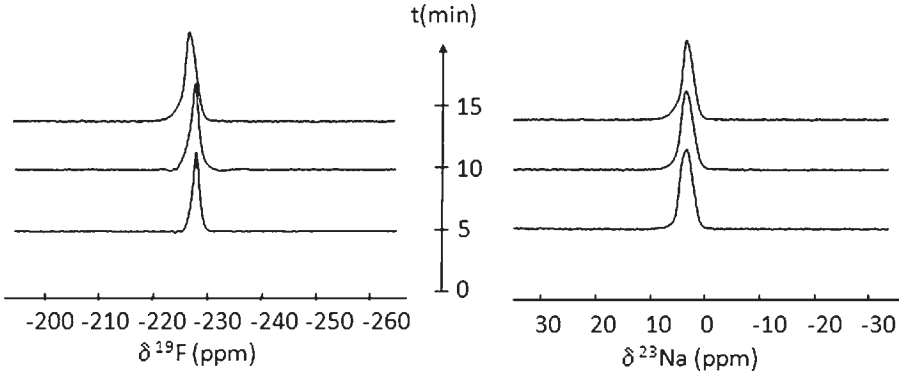

Figure 4. ^{19}F and ^{23}Na NMR spectra of NaF at 1283 K. The spectra were registered over 15 min at the same temperature to control any possible evolution of the melt.

dx.doi.org/10.1021/ic1019845 |Inorg. Chem. 2011, 50, 3304–3312

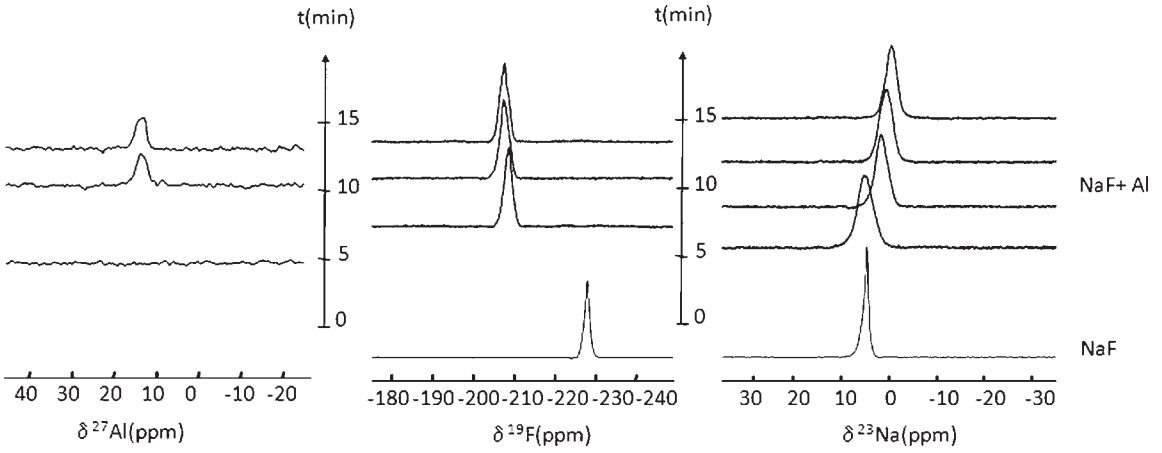

Figure 5. ^{27}Al, ^{19}F, and ^{23}Na NMR spectra at 1283 K in pure NaF and in NaF with Al metal.

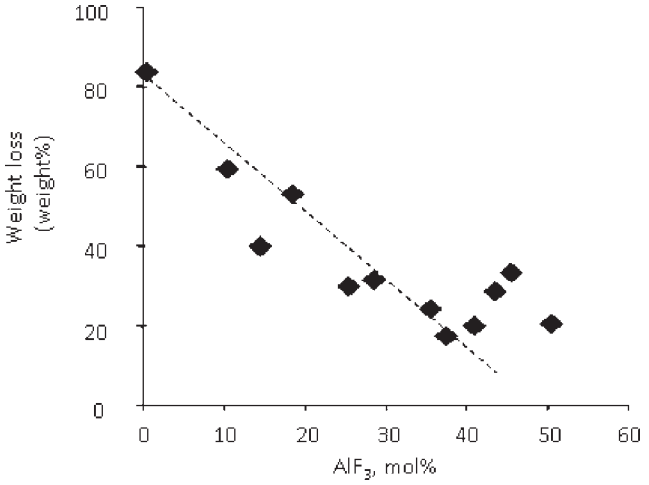

Figure 6. Metal weight loss variation versus AlF_3 content.

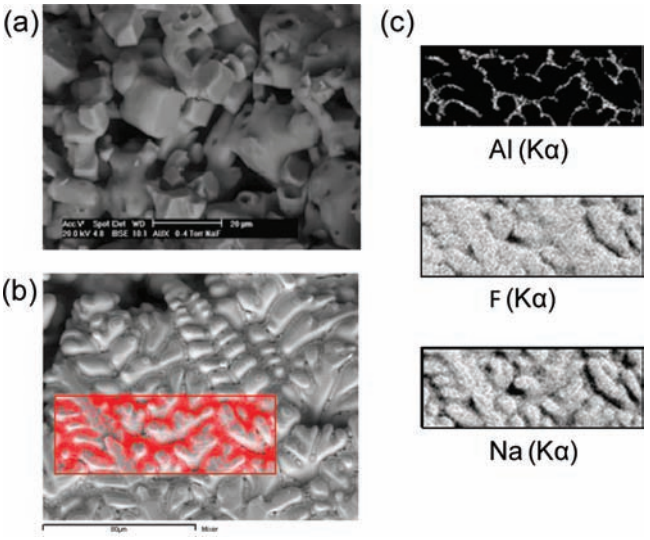

Figure 7. ESEM pictures of NaF (a) and NaF+Al (b) solidified melts with X-ray cartography (c) of the selected area (in red).

effect corresponds to the chemical reaction of the aluminum metal with fluorides of the bath implying an AlF_3 enrichment of the composition, and thus to a modification of the AlF_x^{3-x} species distribution.

For the baths containing Al metal and with higher content in AlF_3 (i.e., above 25 mol % AlF_3) the very slight changes of the chemical shifts' values observed for all nuclei (^{27}Al, ^{19}F, and ^{23}Na) evidence that the chemical reaction with Al metal is less significant than for compositions with higher NaF content.

2.2. Solidified Samples. The samples have been further characterized at room temperature after rapid cooling. The color of the sample varied from dark gray to white, depending on the composition. Three visible domains are detectable in the sample: the position of the aluminum piece, the zone around, and the bath. The metal was extracted to estimate its weight loss. It was observed (Figure 6) that the weight loss decreases with AlF_3 content, as it has been described in the literature.[2,6,7,9] A large deviation was noticed for compositions with higher AlF_3 content (more than 40 mol %). In these samples the aluminum was partly lost under small metallic particles dispersed all over the bath. Thus, it can explain important dispersion values noticed in the weight losses estimated for high AlF_3 content.

ESEM Study of NaF and NaF+Al. For NaF sample, the ESEM picture (Figure 7a) shows a structure with cubic grains linked together. The equiaxial shape of grains indicates a uniform distribution of crystallization germs in the liquid phase and an isothermal cooling of the entire bulk of the sample.

For NaF +Al metal (Figure 7b) mainly a dendritic type structure with a secondary phase localized around the dendrites was observed. Additionally, X-ray mappings of the three elements (Al, F, and Na) of this area (Figure 7c) have been collected and show that the dendrites contain only F and Na, and thus correspond to the NaF phase. The secondary phase is composed of F, Na, and Al. Further analysis by X-ray diffraction, collected at room temperature, brings out the presence of cryolite. Thus, it was concluded that the phase formed around the dendrites is cryolite.

MAS NMR Study of NaF and NaF+Al Metal. The qualitative and quantitative identification of the solid phases present in our solidified samples were made in reference to the ^{19}F, ^{23}Na, and ^{27}Al MAS NMR spectra of NaF, Cryolite, Chiolite, and α-AlF_3 (Tables 1, 2, and 3), recorded in the same conditions.

In NaF, all sodium and fluorine atoms are 6 coordinated.[30] The crystallographic structure of cryolite Na_3AlF_6,[31] a "mixed-cation fluoride perovskite", is monoclinic and made of alternating

dx.doi.org/10.1021/ic1019845 |*Inorg. Chem.* 2011, 50, 3304–3312

Table 1. ^{19}F Isotropic Chemical Shifts[a] of Solids Compounds of NaF-AlF_3 System

compound	site	δ_{iso}/ppm	ref.
NaF	FNa_6^{5+}	−225	this study
		−221	13
Na_3AlF_6	FNa_3Al^{5+}	−190	this study
		−189	13
$Na_5Al_3F_{14}$	FNa_3Al^{5+}	−187	this study
		−187	13
		−189.5	36
	FNa_4Al^{6+}	−191.3	this study
		−190	13
		−191.4	36
	FAl_2^{5+}	−166	this study
		−162	13
		−165	36
α-AlF_3	FAl_2^{5+}	−173	this study
		−174	13
		−172	38

[a] Referenced to $CFCl_3$ 1M.

Table 2. ^{23}Na Isotropic Chemical Shifts, δ_{iso},[a], Quadrupolar Coupling Frequencies, ν_Q, Asymmetry Parameters, η, of Solids Compounds of NaF-AlF_3 System

compound	site	δ_{iso} /ppm	ν_Q /kHz	η	ref.
NaF	NaF_6^{5-}	7.6	200	0	this study
		7	47	0	13
Na_3AlF_6	NaF_6^{5-}	2.2	240	0	this study
		4	450	1	39
		2	420	0.6	37
		1	240	0	13
	NaF_8^{7-}	−8	700	0.28	this study
		−8	725	0.25	39
		−9	715	0.3	37
		−12	700	0.28	13
$Na_5Al_3F_{14}$	NaF_6^{5-}	−7	1600	0.12	this study
		−6	1600	0.15	39
		−9	1590	0.1	37
		−7	1600	0.12	13
	NaF_{12}^{11-}	−20.5	770	0	this study
		−21	750	0	39
		−24	740	0	37
		−21	770	0	13

[a] Referenced to NaCl 1M.

AlF_6^{3-} and NaF_6^{5-} octahedra while the Chiolite, $Na_5Al_3F_{14}$, has a tetragonal structure[32−34] with alternating layers of AlF_6^{3-} octahedra linked by their tops and layers of NaF_6^{5-} octahedra linked by their edges, the sodium being located between the layers.[37] Two different types of AlF_6^{3-} are present in the structure: $Al_{[1]}F_6^{3-}$ at the center of an axially symmetric octahedron with in-plane Al−F distances of 1.795 Å, and $Al_{[2]}F_6^{3-}$ located in a more distorted octahedron with in-plane Al−F distances of 1.789 Å. The corresponding ^{27}Al signals differ by the chemical shifts values but also mainly by the quadrupolar couplings and the associated complex lineshapes.

Table 3. ^{27}Al Isotropic Chemical Shifts, δ_{iso},[a], Quadrupolar Coupling Frequencies, ν_Q, Asymmetry Parameters, η, of Solids Compounds of NaF-AlF_3 System

Compound	Site	δ_{iso} /ppm	ν_Q /kHz	η	ref.
α-AlF_3	AlF_6^{3-}	−16.5	120	0	this study
		−16	4.8	0	37
		−15	0	0	13
Na_3AlF_6	AlF_6^{3-}	0	80	0	this study
		0	90	0.9	37
		−1	70	0	13
		0	90	0	39
$Na_5Al_3F_{14}$	$Al_{[1]}F_6^{3-}$	−1.5	1150	0.13	this study
		−4	1200	0.15	37
		−1.5	1200	0.13	13,33
		−1	1185	0	39
	$Al_{[2]}F_6^{3-}$	−2.8	900	0	this study
		−9	880	0	37
		−2.8	900	0	13,33
		−3	900	0	39

[a] Referenced to $Al(NO_3)_3$ 1M.

In the case of the NaF+Al sample, the ^{19}F MAS NMR spectrum shows clearly the presence of two signals corresponding to NaF and cryolite (Figure 8a) at −225 ppm and −189 ppm,[13] in good agreement with the values reported by Lacassagne et al.[13] It is also confirmed in ^{23}Na MAS NMR spectrum (Figure 8b) with the signal of NaF at 7 ppm and the two peaks corresponding to the two Na sites in cryolite: NaF_6^{5-} at 2 ppm[37] and NaF_8^{7-} at −8 ppm.[39] The ^{27}Al MAS NMR spectrum for this solidified sample (Figure 9) evidences two ^{27}Al signatures: at 0 ppm corresponding to cryolite and at 1650 ppm for aluminum metal. The detection of the signal of metallic aluminum at 1650 ppm is associated with the presence of very small metallic particles ($\phi < 50\,\mu$m). It coincides with the important weight loss measured for the aluminum piece in this sample.

MAS NMR Study of NaF-AlF_3 and NaF-AlF_3-Al Systems. The relative proportion of each phase has been defined from the intensities of the different signals (Figure 10). When aluminum metal is added in the NaF-AlF_3 system, starting from its formation in NaF sample, the proportion of cryolite is systematically higher than in samples without metal. In the same way, chiolite is detected at lower AlF_3 content. This evolution indicates a chemical reaction between the metal and the melt leading to an increase of the AlF_3 content in the bath. This reaction is also strongly dependent on the composition and on the acidity of the melt. For compositions with AlF_3 content higher than 37.5 mol %, no variation was observed.

From the ^{27}Al MAS NMR spectra, for 0−25 mol % AlF_3 range, when AlF_3 content increases, it is observed that the intensity of the Al metal signal at 1650 ppm decreases. This tendency can be due either to metallic dispersions that disappear by reaction with the bath or to the presence of bigger particles which are difficult to be detected by NMR. For compositions with high AlF_3 content, no metal signal has been detected on ^{27}Al MAS NMR spectra. Nevertheless, a large signal is observed at 70 ppm with a typical quadrupolar line shape which can be assigned to the signal of alumina. The formation of alumina can be associated with the oxidation of the sample during grinding procedure, this oxidation being directly

dx.doi.org/10.1021/ic1019845 |*Inorg. Chem.* 2011, 50, 3304–3312

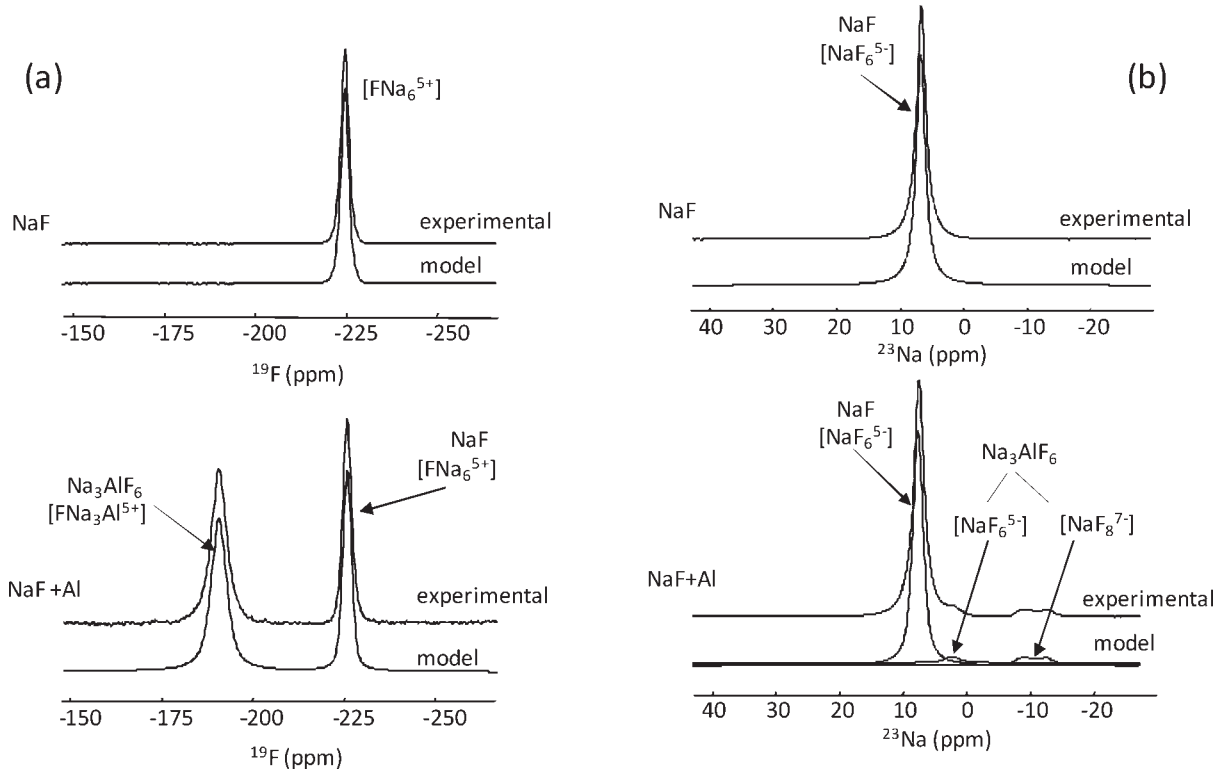

Figure 8. ^{19}F (a) and ^{23}Na (b) MAS NMR spectra of NaF and NaF+Al.

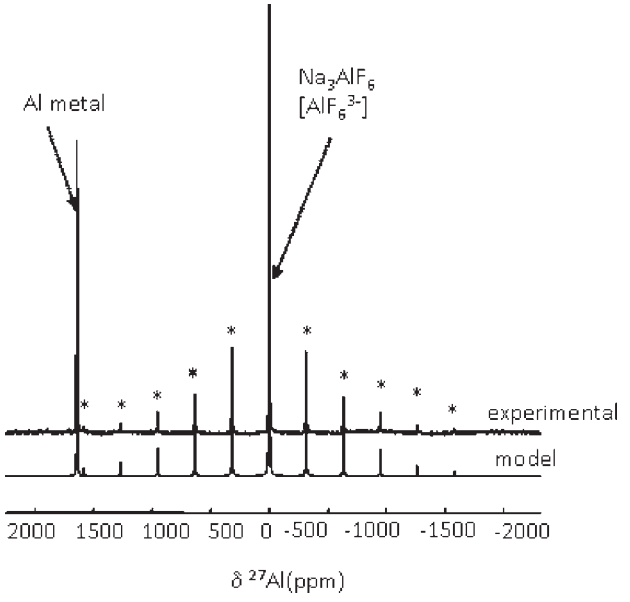

Figure 9. ^{27}Al MAS NMR spectra of NaF+Al. Asterisks, *, designate spinning sidebands.

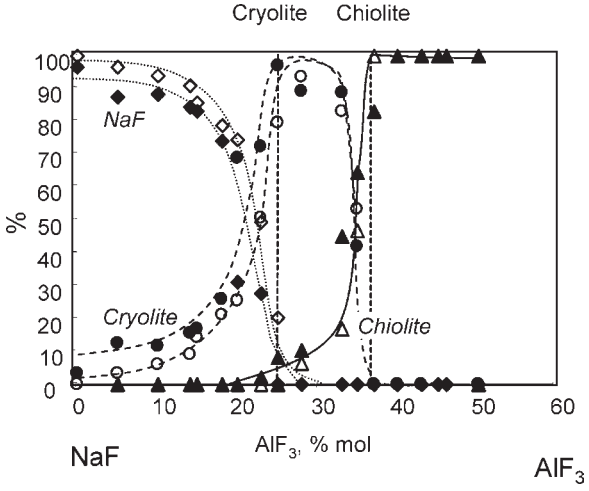

Figure 10. Relative proportions of the different solid phases (NaF, Cryolite, and Chiolite) extracted from ^{23}Na MAS NMR spectra intensities for NaF-AlF_3 and NaF-AlF_3-Al systems. ◊ NaF, ○ cryolite, Δ chiolite: filled symbols with Al, empty symbols without Aluminum.

connected with of the existence of large metallic particles in the mixture.

2.3. Influence of the Cation. To confirm these observations, we have tested the influence of metallic aluminum in pure molten LiF and KF. To enhance the possible reactions over the whole sample, we have mixed the fluorides sample with aluminum powder (ϕ 15 μm), using the same proportions than in the previous description. In the case of potassium fluoride, a ^{27}Al signal is also visible after few minutes in the melt at 28 ppm, a chemical shift intermediate between the one measured in molten K_3AlF_6 (22 ppm) and $KAlF_4$ (43 ppm). In molten LiF no ^{27}Al signal has been detected even after 15 min. Figure 11 reports the ^{27}Al NMR spectra obtained in molten KF and NaF with aluminum additions compared with the signals measured in molten M_3AlF_6 and $MAlF_4$ (M = K, Na). We can argue for a stronger reactivity in the KF system. The signal position corresponds to chemical shifts associated with lower average coordination and consequently to a higher amount of AlF_4^- species in the melt.

dx.doi.org/10.1021/ic1019845 |Inorg. Chem. 2011, 50, 3304–3312

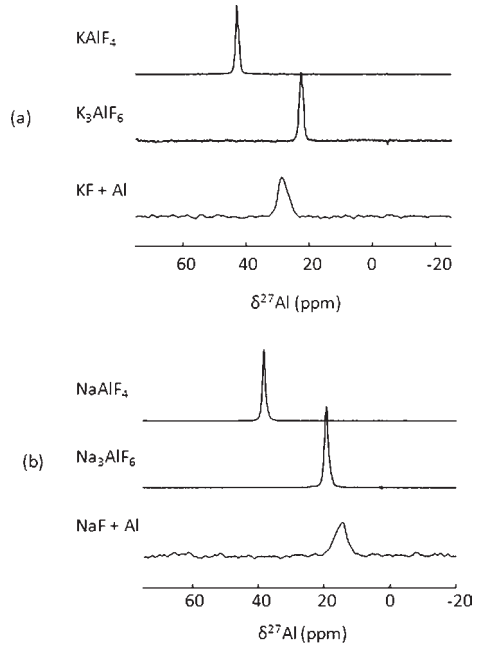

Figure 11. ^{27}Al NMR spectra of KF (a) and NaF (b) mixed with aluminum powder and compared with the corresponding ^{27}Al spectra in molten M_3AlF_6 and $MAlF_4$ (M = K, Na).

3. CONCLUSION

The high temperature NMR approach of the interactions occurring between metallic aluminum and the melts of the binary system NaF-AlF_3 provides a unique way to visualize the reactions existing at the interface between the aluminum and the cryolitic bath in aluminum electrolysis.

In the literature the description of such reactions were often deduced from observations at room temperature after rapid cooling of the melt. Nevertheless even if some dispersions are detected in the solidified melt, the size of such particles is strongly dependent on the cooling rate and the composition.

By the combination of the ^{19}F, ^{23}Na, and ^{27}Al NMR chemical shifts observations we are able to describe in situ the effect of aluminum dissolution over a wide range of composition.

We have shown the modification of the distribution of fluoroaluminate species in the bath with metallic addition depending on AlF_3 content. Addition of metallic aluminum in pure NaF leads to the formation of fluoroaluminate species in the melt, according to the ^{27}Al chemical shift value. For low AlF_3 contents (below 25 mol %), the important effect on ^{19}F and ^{27}Al chemical shifts illustrates the strong reaction between the aluminum metal and these melts. The characterization of the solidified mixtures at room temperature by NMR and ESEM confirmed this AlF_3 enrichment of the baths.

For composition with higher AlF_3 content, no modification of the NMR spectra indicated that no reaction between the metal and the baths occurred.

The ^{27}Al NMR signature of the metallic aluminum under 25 mol % AlF_3 indicates that aluminum is present under small particles disseminated in the sample. For higher contents in AlF_3, the signature of the metal is not direct but is expressed by the presence of alumina. These observations are confirmed by microscopy with the observation of large particles of aluminum more or less oxidized. These results are of major importance for the aluminum industry and allow a better understanding of the speciation and of the chemical properties of the electrolytic bath.

AUTHOR INFORMATION

Corresponding Author

*E-mail: bessada@cnrs-orleans.fr. Fax: [+33] (0) 238 63 81 03.

Present Addresses

[§]Now at SIMAP, CNRS UMR 5266, 1130 rue de la Piscine BP 75, 38402 St Martin d'Hères Cedex, France.

ACKNOWLEDGMENT

The authors acknowledge Sylvie Bouvet from Rio-Tinto-Alcan for the Aluminum samples. I.N. thanks the CNRS and the Region Centre for financial support. The authors thank Dr. Aydar Rakhmatullin for his help and advices in high temperature NMR experiments.

REFERENCES

(1) Thonstad, J., Fellner, P., Haarberg, G. M., Hives, J., Kvande, H., Sterten, A. *Aluminum Electrolysis*, 3rd ed.; Aluminum Verlag: Düsseldorf, Germany, 2001.

(2) Grjotheim, K., Krohn, C., Malinovsky, M., Matiakovsky, K., Thonstadt, J., *Aluminum Electrolysis. Fundamentals of the Hall-Héroult Process*, 2nd ed.; Aluminum-Verlag: Düsseldorf, Germany, 1982.

(3) Kvande, H. *Light Met.* **1980**, 171–174.

(4) Thonstad, J.; Oblakowski, R. *Electrochim. Acta* **1980**, *25*, 223–227.

(5) Zhuxian, Q.; Liman, F.; Grojtheim, K.; Kvande, H. *J. App. Electrochem.* **1987**, *17*, 707–714.

(6) Haarberg, G. M.; Støre, T.; Thonstadt, J.; Pietrzyk, S.; Silny, A. *Proceedings of the 10th Slovakian-Norvegian Symposium on Aluminium Smelting Technology*, Stara Lesna, Slovakia, Sept 21−23, 1999.

(7) Haupin, W. E. *Light Met.* **1999**, 395–398.

(8) Prasad, S. *J. Braz. Chem.Soc.* **2000**, *11* (3), 245–251.

(9) Haarberg, G. M.; Thonstadt, J.; Pietrzyk, S.; Egan, J. J. *Light Met.* **2002**, 1083–1088.

(10) Kvande, H. *High Temp.-High Pressures* **1982**, *14*, 245–252.

(11) Kvande, H. *High Temp.-High Pressures* **1983**, *15*, 51–62.

(12) Auguste, F. Ph.D. Thesis, Liège University, Belgium, 1998.

(13) Lacassagne, V.; Bessada, C.; Florian, P.; Bouvet, S.; Ollivier, B.; Coutures, J. P.; Massiot, D. *J. Phys. Chem. B* **2002**, *106*, 1862–1868.

(14) Nuta, I.; Bessada, C.; Veron, E.; Matzen, G. *C. R. Chim.* **2004**, *7*, 395–400.

(15) Bonafous, L.; Ollivier, B.; Auger, Y.; Chaudret, H.; Bessada, C.; Massiot, D.; Farnan, I.; Coutures, J.-P. *J. Chim. Phys.* **1995**, *92*, 1867–1870.

(16) Bennett, A. E.; Rienstra, C. M.; Griffiths, J. M.; Zhen, W. G.; Lansbury, P. T.; Griffin, R. G. *J. Chem. Phys.* **1998**, *108* (22), 9463–9479.

(17) Ernst, M. *J. Magn. Reson.* **2003**, *162* (1), 1–34.

(18) Massiot, D.; Fayon, F.; Capron, M.; King, I.; Le Calvé, S.; Alonso, B.; Durand, J. O.; Bujoli, B.; Gan, Z.; Hoatson, G. *Magn. Reson. Chem.* **2002**, *40*, 70–76.

(19) Gilbert, B.; Materne, T. *Appl. Spectrosc.* **1990**, *44* (2), 299–305.

(20) Robert, E.; Lacassagne, V.; Bessada, C.; Massiot, D.; Gilbert, B.; Coutures, J.-P. *Inorg. Chem.* **1999**, *38*, 214–217.

(21) Gilbert, B.; Robert, E.; Tixon, E.; Olsen, J. E.; Ostvold, T. *Inorg. Chem.* **1996**, *35*, 4198–4210.

(22) Kohn, S. C.; Dupree, R.; Morutza, M. G.; Henderson, C. M. B. *Am. Mineral.* **1991**, *76*, 309–321.

(23) Dirken, P. J.; Jansen, J. B. H.; Schuiling, R. D. *Am. Mineral.* **1992**, *77*, 718–724.

(24) Tixhon, E.; Robert, E.; Gilbert, B. *Appl. Spectrosc.* **1993**, *48*, 1477–1482.

(25) Gilbert, B.; Robert, E.; Tixon, E.; Olsen, J. E.; Ostvold, T. *Light Met.* **1995**, 181–186.
(26) Robert, E.; Olsen, J. E.; Gilbert, B.; Ostvold, T. *Acta Chem. Scand.* **1997**, *51*, 379–386.
(27) Knight, W. D. *Solid State Physics*; Seitz, F., Turnbull, D., Eds.; Academic Press Inc.: New York, 1956; Vol. 2, p 93.
(28) MacKenzie, K. J. D.; Smith, M. *Multinuclear solid-state NMR of Inorganic Materials*, Pergamon Materials Series; Elsevier Science: New York, 2002.
(29) Drain, L. E. *Metall. Rev.* **1967**, *12* (119), 195–228.
(30) Deshpande, V. T. *Acta Crystallogr.* **1961**, *14*, 794–794.
(31) Hawthorne, F. C.; Ferguson, R. B. *Can. Miner.* **1975**, *13*, 377–382.
(32) Jacoboni, C.; Leble, A.; Rousseau, J. J. *J. Solid State Chem.* **1981**, *36* (3), 297–304.
(33) Lacassagne, V.; Florian, P.; Montouillout, V.; Gervais, C.; Babonneau, F.; Massiot, D. *Magn. Reson. Chem.* **1998**, *36* (12), 956–959.
(34) Dutour, J.; Guillou, N.; Huguenard, C.; Taulelle, F.; Mellot-Draznieks, C.; Férey, G. *Solid State Sci.* **2004**, *6* (10), 1059–1067.
(35) Kissel, D. *J. Fluorine Chem.* **1984**, *24*, 327–340.
(36) Du, L. S.; Samoson, A.; Tuherm, T.; Grey, C. P. *Chem. Mater.* **2000**, *12*, 3611–3616.
(37) Silly, G.; Legien, C; Bizare, Y. Y; Cavayac, F. *Solid State NMR* **2004**, *25*, 241.
(38) Chan, J. C. C.; Eckert, H. *J. Non-Cryst. Solids* **2001**, *284*, 16–21.
(39) Spearing, D. R.; Stebbins, J.; Farnan, I. *Phys. Chem. Miner.* **1994**, *21*, 373–386.